ScienceAdvances

www.advances.sciencemag.org/cgi/content/full/1/3/e1500036/DC1

Supplementary Materials for

Crowdsourced earthquake early warning

Sarah E. Minson, Benjamin A. Brooks, Craig L. Glennie, Jessica R. Murray, John O. Langbein, Susan E. Owen, Thomas H. Heaton, Robert A. Iannucci, Darren L. Hauser

Published 10 April 2015, *Sci. Adv.* **1**, e1500036 (2015)
DOI: 10.1126/sciadv.1500036

This PDF file includes:

Crowdsourced Earthquake Early Warning

Supplemental Material

1. Operational Early Earthquake Warning

EEW is the subject of active research in many parts of the world. There are few regions, however, where EEW systems are currently operating and sending information to users other than the researchers developing the warning system (Fig. 1). EEW operates throughout Japan and Taiwan. In Mexico, the cities of Mexico City, Oaxaca City, Toluca, Chilpancingo, Acapulco, and Morelia currently receive warnings (Juan Manual Espinosa Aranda, Shri Vishna Singh, Carlos Valdes, personal communication, 2014). Warnings are sent to the Marmara region of Turkey including Istanbul province (Erdik Mustafa, personal communication, 2014). Four nuclear power plants in Switzerland currently receive warnings (John Clinton, personal communication, 2014) as do assorted nuclear facilities, dams, and public and private emergency responders in Romania (Constantin Ionescu, personal communication, 2014). An EEW system has recently begun operating in the Chengdu region of China (Tun Wang, personal communication, 2014.) Finally, while an EEW system is currently in beta testing for most of the west coast of the United States including California, Oregon, and Washington, at present only California has external users of the U.S. EEW system. All of these EEW systems utilize seismic data only, although GNSS data are beginning to be incorporated into the U.S. and Japanese EEW systems (Yusaku Ohta, personal communication, 2014) and the Mexico system will soon use GNSS data as well (Juan Manual Espinosa Aranda, Shri Vishna Singh, Carlos Valdes, personal communication, 2014). Background color in Fig. 1 is peak ground acceleration with 10% probability of exceedance in 50 years given a 475 year return period from the Global Seismic Hazard Assessment Program. Most regions of the world with high seismic hazard have no EEW capabilities (Fig.1).

2. Empirical Noise Characterization

We assess a typical smartphone's capability to detect permanent surface displacements by first empirically characterizing positioning noise from a variety of different consumer GNSS receivers (including those found in Google Nexus 5 smartphones, first-generation Apple iPad tablets, u-blox receivers, and Garmin eTrex handheld receivers) as well as Japan's GEONET GNSS receivers. All GNSS data analyzed are coarse acquisition (C/A) code (*19*). For the time periods most pertinent to EEW application (seconds to tens of seconds), we find that noise character depends both on the device model version and whether it is stationary or moving (Fig. S1-S2). When stationary, epoch-to-epoch repeatability (the ability to recover position at each epoch) for modern devices (e.g., Nexus 5) is ~0.01-0.02 m and for older devices it is less than ~1 m (e.g., iPad) (Fig. S1). When moving at a constant velocity, the Nexus 5 repeatability is ~1.5 m (Fig. S1). This strongly suggests that, when stationary, the Kalman filter onboard the smartphone assumes an essentially constant velocity model – an assumption that would hold for most pedestrian navigation applications where it would be desirable to minimize accelerations due to bodily motion or device manipulation.

The repeatability for all of these devices depends upon the time-span of the measurements because they all have background noise that exhibits temporal correlations (i.e., the noise spectra are "red"). Consequently, the time series of position estimates exhibit drift that we assess following (*31*) (Fig. S2). At intervals of a few seconds, the raw C/A code positions can resolve displacements of 10 cm; but for longer intervals (e.g., 60 seconds), their sensitivity decreases to 2-3 m. (Note that there is less drift in positions estimated from C/A code data recorded at GEONET GPS stations than from C/A code data recorded on a consumer receiver. This is because scientific GPS stations have higher quality hardware. The most significant difference is probably the reduction in multipathing made possible by

the choke ring antennas at scientific GPS sites.) Satellite Based Augmentation System (SBAS) corrections or phase smoothing significantly improves the precision of the consumer devices by a factor or 10 or more.

3. Offset Tests

As discussed in the main text, we subjected the platform to a series of displacements ranging from ~0.1-2.0 m (Fig. 2, S3**)** and find that the raw C/A positions (with SBAS) faithfully records the entire displacement range. In contrast, the smartphone is essentially insensitive to the displacements because its onboard data processing uses a Kalman filter that removes most of the external motion to which the device was subjected.

To assess the full potential of consumer grade GNSS and INS devices for earthquake monitoring, we constructed our own extended Kalman filter using raw C/A code data from the u-blox receiver and accelerometer data from the Nexus 5. The Kalman filter uses a constant jerk state space model for system dynamics (*21*). Given GNSS positions and three-component accelerometer observations, the filter simultaneously estimates displacement and accelerometer bias. Fig. 2A in the main text shows the results of a 50 cm offset test and demonstrates that the Kalman filtered solution could accurately recover the displacement time history to which the receiver was subjected even though the twice-integrated (yielding displacement) accelerometer record demonstrates a large amount of drift over earthquake time-scales.

4. Earthquake Monitoring Capabilities of Consumer Devices

Fig. 2B compares the empirical drifts we estimated for a variety of instruments (Fig. S2) with observed displacement time series for recent notable damaging earthquakes (Table S1) (*22, 23, 25*). The strong motion accelerometer drift was estimated by differencing a twice-integrated observation of the 2011 Tohoku-oki earthquake recorded on the east component of K-net strong motion station MYG011 and a corresponding displacement time series from nearby GEONET GPS station 0550. The consumer accelerometer drifts were obtained by averaging at 62,225 observation locations the absolute value of the difference between ground motion time series from the M_w 7 Hayward fault scenario and twice-integrated corresponding simulated acceleration time series using noise from a Nexus 5 smartphone's onboard accelerometer. Similarly, the Kalman filter drift time series were obtained by averaging at those same observation locations the absolute value of the difference between the ground motion time series and corresponding simulated Kalman filter time series computed by combining the same acceleration records with simulated C/A code GNSS time series in the same manner as Section 4. These simulated time series were originally 90 sec duration and then extrapolated from 90 sec to 100 sec. Both the simulated and empirical noise time series were smoothed for plotting purposes. Note that noise characteristics for data involving accelerometer observations are very sensitive to the type of motion to which the instrument was subjected. This can be clearly seen for the Kalman filter drift curve which was calculated for an M_w 7 earthquake. Once the ground shaking ceases, the Kalman filter acts to damp further drift of the estimated displacement.

Figure 2C shows the minimum magnitude observable (as a function of distance) with a signal-to-noise ratio (SNR) of at least 10 for the devices in Fig. 2B. The SNR for displacement observations was computed by assuming that the signal is the peak ground displacement (PGD) as a function of magnitude and distance (*27*), which we assume occurs at approximately the S-wave arrival time. Thus the noise is the amount of drift that accumulates between the P-wave arrival and S-wave arrival assuming wave speeds of 6 km/s and 3.5 km/s, respectively, where the drift accumulation follows the

curves shown in Fig. 2B. The SNR curve for the acceleration observed by a consumer accelerometer was computed by assuming the amplitude of the signal was given by the peak ground acceleration (PGA) (*27*), and that the noise over short time durations was Gaussian with an amplitude of 0.031 m/s^2 based on the noise characteristics we observed over short time periods for the accelerometer in a Nexus 5 smartphone. As in Fig. 2B, the curves in Fig. 2C were smoothed for plotting purposes.

5. Hayward Fault Rupture Simulation

We simulated a crowdsourced EEW response to a scenario magnitude 7 earthquake on California's Hayward fault using two different types of data. In the main text (Fig. 3), we presented results from assuming that different fractions of the population contributed data from consumer devices containing both an accelerometer and a simple GNSS C/A code receiver equipped with neither SBAS differential corrections nor phase-smoothed L1 data. (Almost all smartphones record acceleration and C/A code data.) We then Kalman filtered the twice-integrated acceleration time series and GNSS position time series, and modeled the resulting displacement estimates. In Fig. S4, we show the results from assuming different fractions of the population contributed data from consumer devices with SBAS-enabled GNSS receivers with phase smoothing but no accelerometer. (This is the highest quality type of GNSS receiver commonly found in consumer devices.) The results in Fig. 3 and Fig. S4 are nearly identical. Both types of positioning data yield earthquake detection in 5 seconds (assuming 0.2% of the population submits usable data), earthquake locations with errors <5 km and very accurate moment magnitude estimates at all times for all levels of participation.

Data Generation

The uncertainties of GNSS vertical positions are typically much worse (at least a factor of two) than horizontal positions (*19*). Accordingly, all of the modeling in this paper was accomplished using only the 2-D horizontal displacements calculated from the east and north position time series.

To simulate the horizontal displacements we would obtain from consumer devices located near the rupture of a moderate magnitude earthquake, we began with the predicted horizontal ground motion time series for the M_w 7 Hayward fault scenario rupture called hs+hn_n04_hypoO_vr92_tr15 (*32*). Smartphone GNSS (raw C/A code) and acceleration records were then simulated by adding to these time series the empirical noise spectra of displacements obtained from a stationary raw C/A code GNSS receiver (Garmin eTrex) (*31*) and the accelerometer on a Nexus 5 smartphone. We then applied a Kalman filter to combine the resulting C/A code and twice-integrated acceleration time series. The choice of the Garmin eTrex is a conservative one as it is the noisiest of all the devices (Fig. S1-S2). We also simulated consumer GNSS data with real-time corrections by adding to the original synthetic displacement time series the noise characteristics we had determined empirically for the stationary u-blox receiver with SBAS and phase smoothing. These two simulated datasets allow us to explore the results obtainable from two hardware configurations we are likely to encounter in a crowdsourced earthquake monitoring system: one that provides GNSS and accelerometer data without SBAS or phase smoothing, and one that provides GNSS data with differential corrections from SBAS.

In the Kalman filter case, we computed east and north component displacement time series with a one second sampling rate from independent Kalman filters using a constant jerk state space model for system dynamics (*21*). Given a position time series and an accelerometer time series, the filter simultaneously estimates displacement and the bias for the accelerometer measurements. This is a dynamic model that accounts for the changes in position, velocity, and acceleration that these devices

will be subjected to during an earthquake. Simulated earthquake displacements only give three degrees of freedom (x, y, and z displacement). For a full inertial system simulation 6 degrees of freedom (3 displacements and 3 rotations) are required. We made the simplifying assumption that the sensitive axes of the accelerometer triad were always aligned with the simulated motion directions of the earthquake. With this assumption, because the accelerometers are mutually orthogonal (as are the simulated displacements), we can treat the x, y, and z displacements separately as three 1-D estimation problems.

Observation locations were chosen to mimic the distribution of data we might obtain if a certain percentage of the population participated in crowdsourced earthquake monitoring. Our approach was to choose a random distribution of land-based observing locations within a 35 km-by-100 km rectangular box centered on the Hayward fault with the number of observations equal to a percentage of the population within that box (Fig. 3, S4). Since only a small fraction of the population might choose to participate in a crowdsourced EEW system and only a small fraction of those participants may be contributing usable data at any given time, we purposefully chose to consider cases where a very small percentage of the population reported observations of the earthquake. Specifically, we considered the cases where we obtained data from 0.0125%, 0.025%, 0.05%, 0.1%, and 0.2% of the population in the 35 km-by-100 km region. These cases correspond to 294, 587, 1174, 2348, and 4696 observations, respectively (Table S2).

Earthquake Detection

At each second, we counted the number of observing devices that detected a trigger where we determined that a device had been triggered if it and the four devices nearest to it each have accumulated a horizontal displacement in excess of 5 cm. This criterion requires that the displacement signal be spatially coherent as we expect earthquake displacements to be. We then declare that an earthquake has been detected when at least 100 observers simultaneously report triggers. This criterion is reached in less time with increasing numbers of observations simply because, with a denser set of observations, the seismic waves do not have to travel as far to reach 100 observers (Table S2).

Locating the Epicenter

At each second after detection, we obtain an earthquake epicenter by fitting a power law to the amplitudes of the horizontal offsets reported by all triggered observers and searching for the source location that minimizes the L1 norm of the residuals (Fig. S5). This estimation is not computationally expensive and so the time required to obtain an epicenter depends on the time required for the displacements to propagate from the earthquake rupture to the receivers. Our errors in the epicenter location are always less than 5 km (Figs. 3, S4).

Note that we use a power law regression of unknown power: $\log A = c_0 + c_1 \log r$, where A is the amplitude of the observed horizontal displacement, r is the distance between the observer and the proposed epicenter, and c_0 and c_1 are the unknown linear regression parameters. Alternatively, we might have fixed $c_1 = -2$ because surface offsets exhibit an r-square decay in the far-field (*5*). However, we are using near-field observations for which the r-square decay does not necessarily hold. Therefore, we solve for the power of the decay in the linear regression.

Determining Earthquake Magnitude

We determine the magnitude at each second by first calculating a finite fault slip model and then computing the moment magnitude associated with that slip model. The finite fault slip models are computed using the Bayesian linear regression approach of (*25*). In that paper, the authors solved for the fault geometry and distributed slip model simultaneously using three-component real-time GPS data. However, here we only have the two horizontal components of motion. Our initial tests indicated that, without the vertical component of deformation, we could not constrain the fault orientation. Instead, we used the accurate epicenter locations obtained to justify assuming that the rupture was located on the Hayward fault, and then assumed a planar fault whose strike and dip represented the average strike and dip of the Hayward fault in the region of the epicenter (strike 325.0000°, dip 76.2309°). (For global application, existing maps of the largest faults would need to be employed.) We sub-divided the fault plane into one row of patches in the down-dip direction and eight patches in the along-strike direction, each patch having a length of 10 km on a side. Our Green's functions were computed for rectangular dislocations in a homogeneous elastic half-space. The moment magnitudes derived from the results of our slip inversion at each second show high accuracy and low latency (relative to the scenario earthquake's actual moment release as a function of time) for all data sets tested (Figs. 3, S4).

6. Tohoku-oki Earthquake Model

Data

As part of routine collection of dual frequency, scientific-grade GPS carrier phase data, the GEONET GNSS stations also record the same pseudorange data that are used for positioning in consumer devices (*19*). To simulate real-time positioning using single frequency data on a consumer device, we estimated positions based only on C/A code pseudorange values on the L1 frequency ("C1" observations) from a selection of GEONET GPS stations (Table S3) using the pr2p (pseudorange to position) algorithm developed by Dr. Mark Miller at JPL as part of the GIPSY-OASIS software package (*33*) (Fig. S6). The algorithm calculates the position and receiver clock bias at each epoch by minimizing a penalty function, the RMS of residuals, for that epoch. An outlier detection algorithm is triggered when the penalty function or individual residuals do not satisfy solution tolerance criteria. The residual threshold for individual pseudorange observations was 40 m, and the RMS pseudorange threshold was 20 m. Once outliers are identified and deleted, the penalty function is minimized again. Broadcast satellite orbits and satellite clock corrections were used. There are no troposphere or ionosphere models applied. The estimation uses the prior epoch's position and receiver clock bias as an initial value for the next epoch's position and clock bias value, but there is no temporal smoothing between position estimates.

Fig. S6 compares the displacement time series from the pr2p processing of the GEONET data for the Tohoku time series to displacement time series obtained through scientific-quality processing that takes advantage of the dual-frequency data these scientific GPS stations collect. At displacements less than 0.5 m, the comparison is degraded by a subset of far-field stations that experienced a spatially confined ionospheric disturbance combined with loss of satellite lock. However, at the vast majority of stations, the offsets estimated from the C/A code and post-processed scientific-grade time series are nearly equal (Fig. S6C).

Earthquake Detection

We use the same method for detecting the Tohoku-oki earthquake as we did for the Hayward fault simulation. However, because the estimated GPS positions include ionospheric noise and spurious jumps due to loss of satellite lock, we increase the minimum horizontal displacement required for

triggering to 75 cm. Further, rather than declaring that an earthquake has been detected when a certain number of triggers have been received, we instead say that we have detected an earthquake when the number of triggers exceeds 5σ relative to the triggering rate during the pre-event period. This accounts for the fact that, at any given time, some subset of GPS stations exhibit spurious displacements. This threshold is reached at 77 sec after the origin time.

Locating the Epicenter

We used the same approach to calculate the earthquake epicenter as we used for the Hayward fault simulation (Fig. S7).

Determining Earthquake Magnitude

At each second, we estimated the total magnitude release for the Tohoku-oki earthquake by estimating a finite fault slip model and calculating the moment magnitude associated with that slip model. We used the same inversion methodology to invert for the slip distribution as we did for the Hayward fault simulation combined with the 1-D layered elastic structure and 3-D curved fault geometry of (*34*). The resulting magnitude release as a function of time closely matches the source-time function obtained by a full kinematic inversion of the Tohoku-oki earthquake rupture using scientific-grade kinematic GPS, static GPS offsets, seafloor geodesy, and both near-field and far-field tsunami data (*24*).

Tsunami Arrival Times

The tsunami arrival times in Fig. 4 were estimated from the time of the first increase in sea level recorded by the ocean-bottom pressure gauges, GPS wave gauges, and coastal tide and wave gauges included in (*28*).

7. Determining Pre-Earthquake Position

Detecting, locating, and modeling the slip distribution of an earthquake requires estimating the observed offset at each second of time relative to the sensor's position prior to the beginning of the coseismic deformation. Note that the later the time of the prior position, the less long-period drift may accumulate between the prior position and the sensor's position during the earthquake. In fact, this prior position need not be from a time before the origin time of the earthquake, only before the first displacement at the sensor's location.

We leave for a future study determining the best way to identify the pre-earthquake position. In this paper, we presented results for earthquake detection from two end-member cases. For the Tohoku-oki earthquake, we used a pre-event position that was estimated from one minute of data observed 1,000 seconds before the current epoch. In contrast, for the Hayward scenario, we used as our prior positions the instantaneous position of each observer at the origin time.

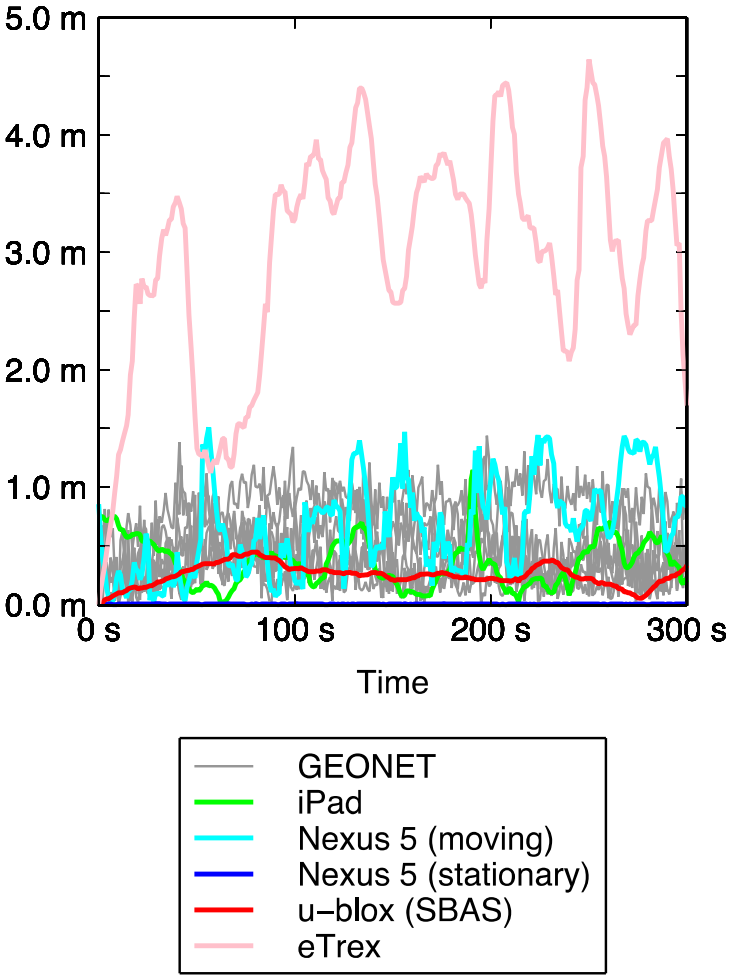

Figure S1. **Background position noise for various GNSS receivers found on consumer devices**. Although each receiver is stationary, there is always some uncertainty in its computed position. The magnitude of the apparent horizontal displacement is shown for position time series computed using C/A code pseudorange-based positioning for six scientific-grade GEONET GPS stations in Japan, a first-generation iPad, a Nexus 5 smartphone, and u-blox and Garmin eTrex consumer GNSS receivers. The position time series for the GEONET stations were computed using the pr2p program, part of the GIPSY-OASIS software package. All other positions were obtained directly from each receiver according to each one's onboard proprietary processing software. Note that the GNSS receiver in the Nexus 5 smartphone applies a Kalman filter to the output position time series and that the parameters of the filter differ depending on whether the receiver appears to be stationary or in motion. The output position time series for both the stationary and moving cases are shown. (For the moving receiver, positions are relative to actual position of the receiver determined from scientific-grade GNSS.) Also, note that the u-blox time series is phase-smoothed and augmented with satellite-based differential corrections (SBAS) that significantly reduce the noise level of its position estimates relative to the other receivers and processing schemes (with the exception of the heavily-filtered positions output by the Nexus 5 in stationary mode).

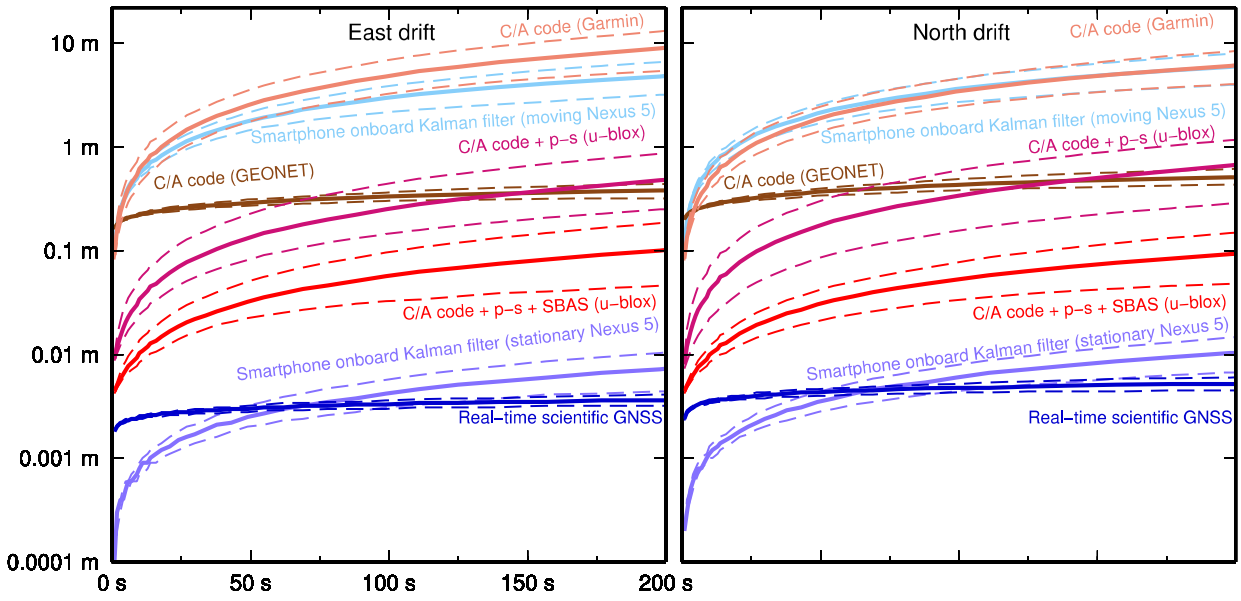

Figure S2. Spectra of drift of position time series for various GNSS receivers found on consumer devices. The drift can be characterized by computing the RMS of $(x(t+\tau)-x(t))$ as a function of various intervals, τ, for position time series obtained as in Fig. S1. Initially, the background noise is quantified by computing a power spectral density (PSD) and further refined by characterizing the PSD as a combination of a power-law and white noise processes. Using the parameters obtained for the power-law and white noise, time series data are simulated and the drift is evaluated to obtain a confidence interval. For each set, the solid line is the nominal RMS of the drift while the dashed lines represent the 95% confidence interval determined from 200 simulations.

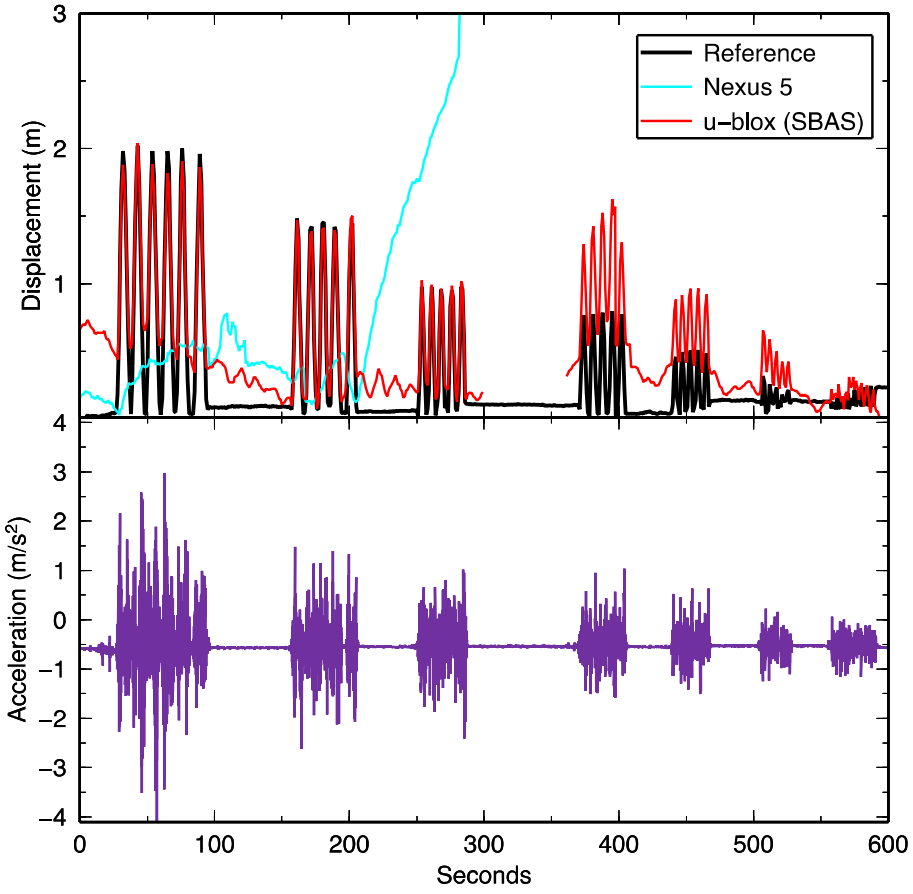

Figure S3. Observed time series from consumer accelerometers and GNSS receivers. Shown are the displacement and acceleration time series obtained from Nexus 5 smartphone and u-blox consumer GNSS receiver when they are subjected to the displacement time history shown in black.

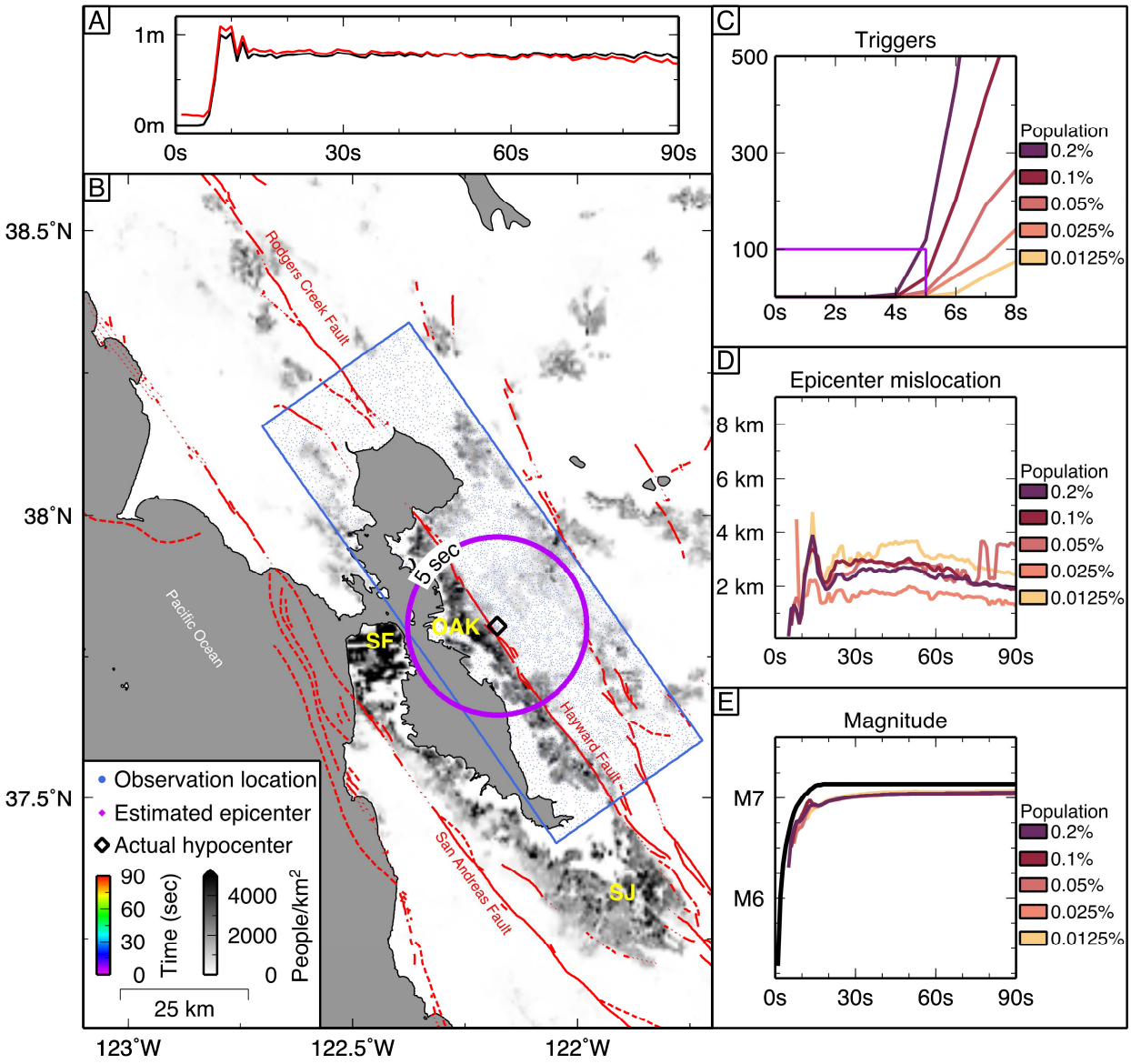

Figure S4. Hayward fault earthquake scenario. Same as Fig. 2 in the main text except simulated consumer-quality GNSS data with SBAS differential corrections and phase smoothing is used instead of Kalman filtered simulated smartphone data. (A) Representative displacement time series from Hayward fault rupture scenario. Black line: true displacement. Red line: simulated smartphone GNSS with SBAS and phase smoothing. (B) Diamonds showing estimated epicentral location colored by time after origin. Contour: S-wave position (assuming 3.5 km/s velocity) when detection criterion is satisfied (5 sec). Yellow text denotes major cities: SF=San Francisco, SJ=San Jose, OK=Oakland. Blue dots denote observer locations assuming 0.2% of the population within the blue box contribute data. (C) Number of observers who have detected a potential earthquake trigger, (D) epicenter location error, and (E) estimated moment magnitude release as a function of time for different levels of participation. Black line in (E) is true magnitude release.

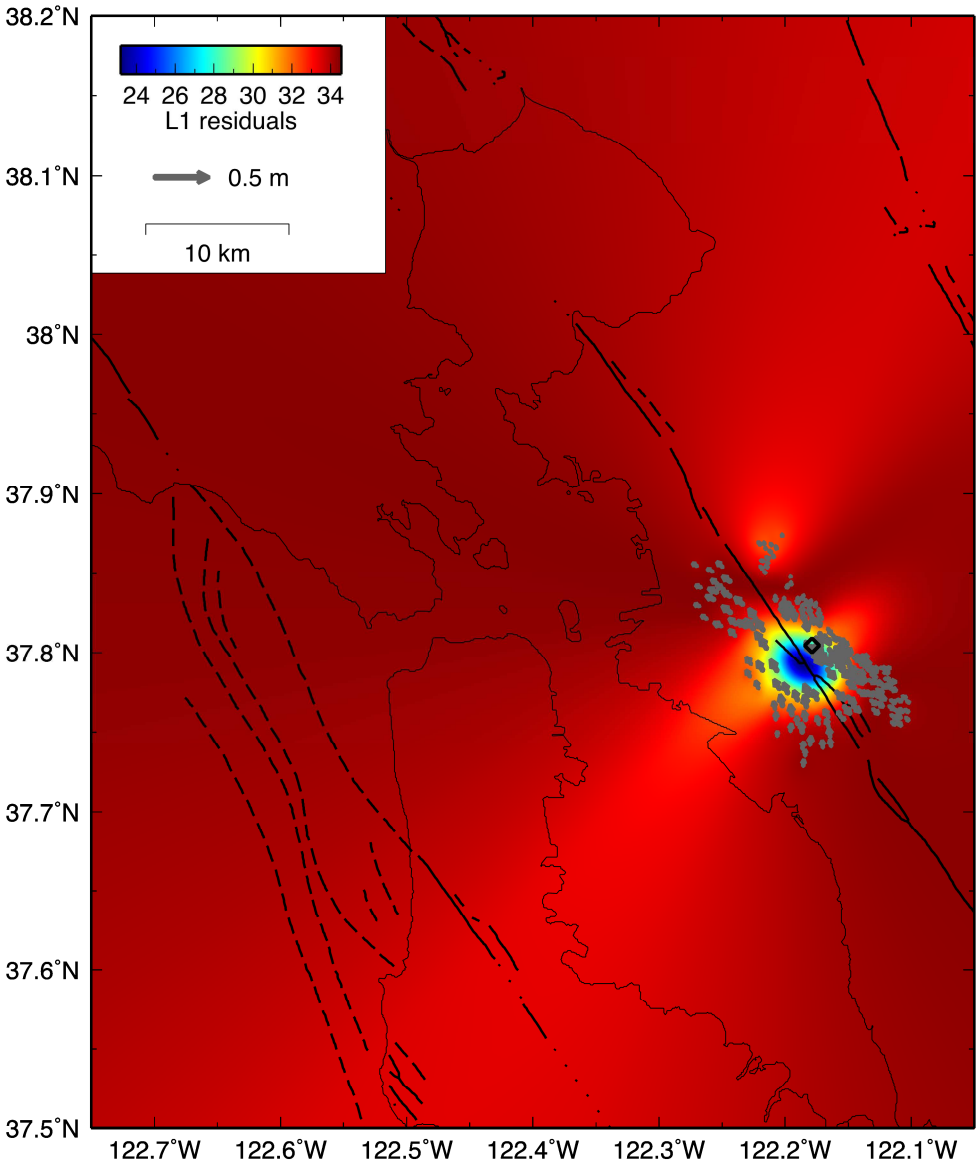

Figure S5. Epicenter location uncertainty for Hayward fault scenario rupture. The observed horizontal displacements at triggered stations 5 sec after the origin time are shown with gray arrows. Background color is the sum of L1 residuals between the log of the amplitude of the observed displacements and the amplitude of the predicted displacements from a power law fit. The location with the lowest residual is inferred to be the epicenter. The black diamond marks the true epicenter. The coastline and major faults are shown in black. The power law fit does a good job of recovering the epicenter location.

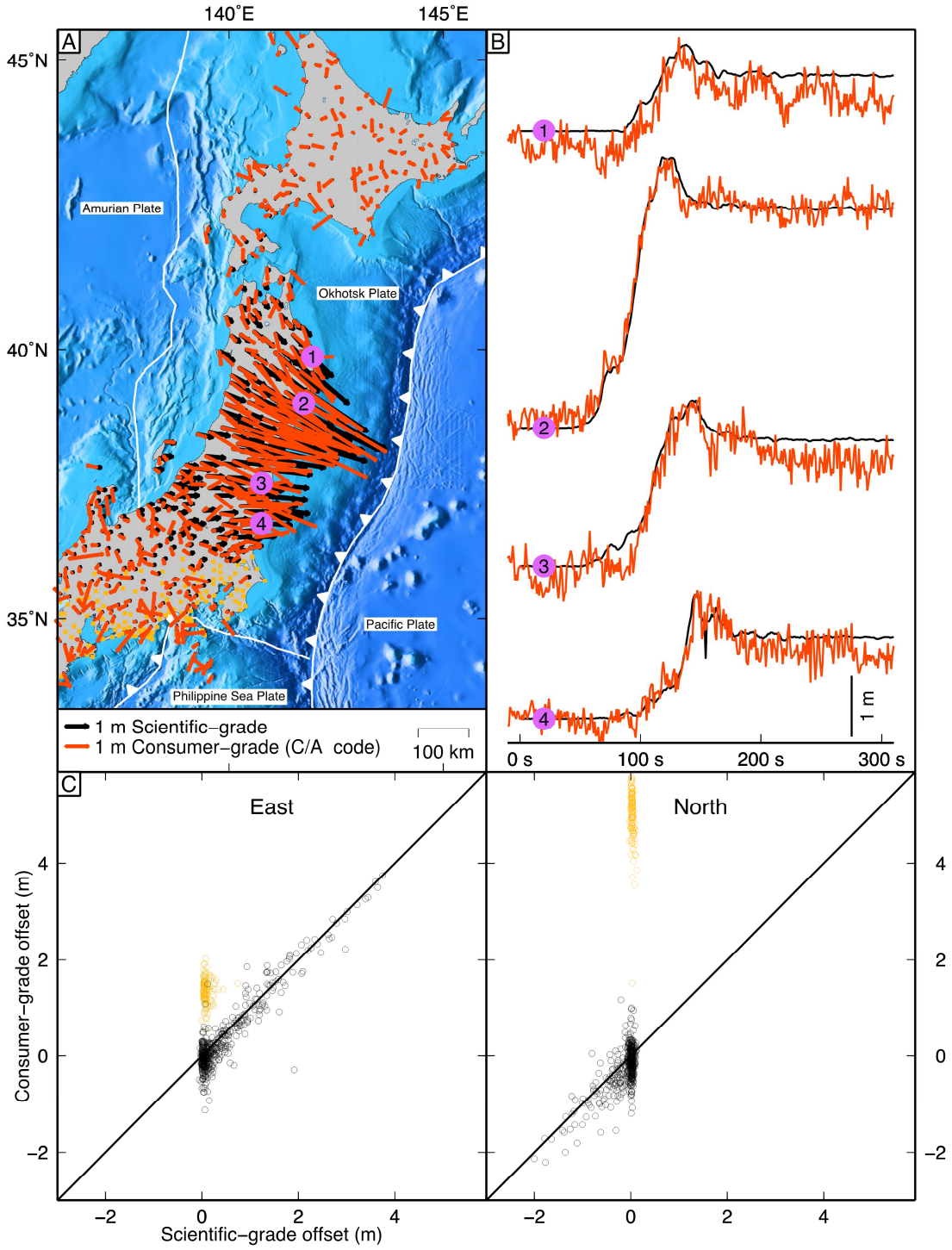

Figure S6. Tohuko-oki earthquake example. (A) Observed static displacements from GEONET stations for Tohoku-oki earthquake. Numbered circles mark locations of time series in (B). Black vectors are offsets estimated from post-processed scientific-grade data. Red vectors are offsets estimated from position time series calculated from observed C/A code data, the same type of positioning found in consumer devices. Yellow squares are locations of stations corrupted by atmospheric noise or loss of satellite lock. (B) Observed east-component time series. Black: scientific-grade post-processed data. Red: consumer-grade (C/A code) data. (C) East and north components of static offsets. Yellow circles correspond to corrupted stations in (A).

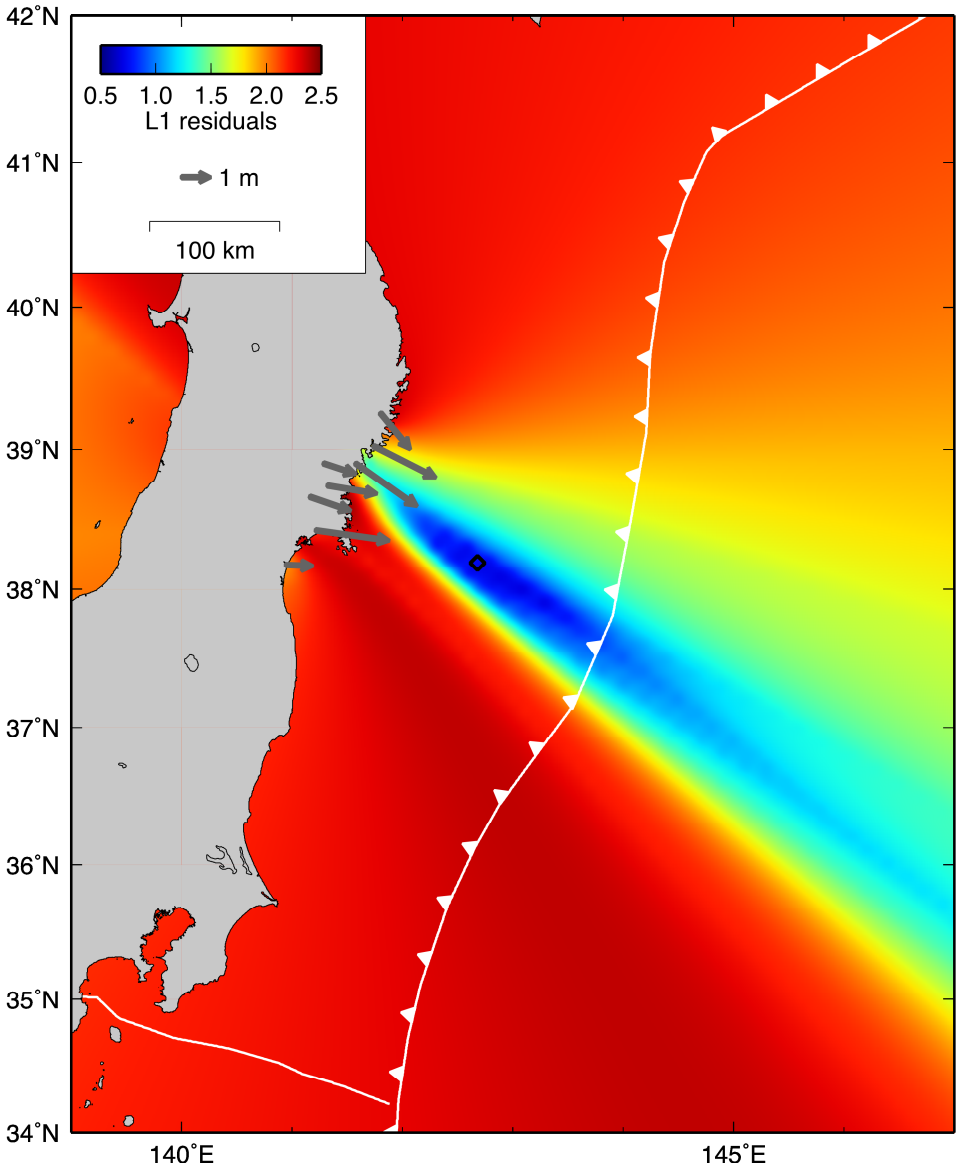

Figure S7. Epicenter location uncertainty for Tohoku-oki earthquake. All colors and symbols are the same as in Fig. S4. Gray arrows are horizontal displacements at triggered stations 100 sec after the origin time. Black diamond is the Tohoku-oki earthquake epicenter (*29*).

Earthquake	M_w	Distance	Station	Component	Description
2011 Tohoku-oki	9.0	76 km	0550	East	Post-processed solution (*24*)
2010 Maule	8.8	70 km	CONS	West	Post-processed solution courtesy of S. E. Owen
2003 Tokachi-oki	8.3	77 km	0015	East	Recreation of real-time processing using a network solution with ultra-rapid orbits and a network adjustment made for each epoch (*22*)
2010 El Mayor-Cucapah	7.2	70 km	P494	South	Real-time solution from the Southern California Earthquake Center available at: http://www.data.scec.org/research-tools/MayorCucapah20100404/
2004 Parkfield	6.0	11 km	HOGS	North	Post-processed solution (*23*)

Table S1. Description of observed GPS earthquake displacement time series shown in Fig. 2B.

Percent of population	Number of observations	Time to reach 100 triggers
0.0125%	294	10 sec
0.025%	587	8 sec
0.05%	1174	7 sec
0.1%	2348	6 sec
0.2%	4696	5 sec

Table S2. Number of data used and detection response times for Hayward fault simulation.

Station	Latitude	Longitude
0001	45.402992	141.750435
0033	38.758595	140.318736
0065	34.465387	136.851128
0002	44.433686	143.224179
0128	42.971378	141.290333
0035	38.331027	140.366086
0251	36.401879	136.920558
0221	36.507995	138.552713
0190	39.327002	140.559778
0160	40.048600	141.461945
0004	43.915690	144.675842
0037	38.317487	140.954184
0252	37.850496	136.919268
0222	36.421628	139.330387
0191	39.206062	139.907717
0130	42.802718	140.603519
0161	39.980574	141.225065
0005	43.507860	144.449008
0283	35.757783	136.975302
0316	33.741273	136.010900
0253	37.446027	137.270049
0223	35.986891	139.075685
0162	39.869370	141.950542
0531	42.982571	144.719147
0131	42.786434	140.233203
0284	35.657189	137.424773
0007	43.589658	142.482479
0102	45.275968	141.038213
0040	37.643696	139.791506
0565	38.023687	138.369882
0255	36.394456	136.388942
0501	45.137712	141.167097
0595	34.737613	139.358585
0193	39.051902	140.629588
0163	39.851246	141.164861
0532	42.125587	143.315695
0132	42.729441	141.863983
0285	35.636153	136.488768
0318	35.466286	136.053666
0103	45.002398	142.537089
0008	43.854011	141.510373
0566	37.535832	138.706939
0041	37.090714	140.902515
0596	34.519633	139.270932

0225	35.657206	140.048093
0164	39.849176	141.803851
0533	41.404706	141.447587
0814	34.719474	138.876472
0781	44.639926	141.793917
0286	35.632897	136.611394
0627	36.103635	140.086307
0104	44.892461	141.741397
0042	36.539928	140.611836
0567	37.348539	138.516369
0257	36.145619	136.278945
0503	44.219722	143.615670
0876	43.240529	141.345959
0597	34.333121	139.210938
0165	39.701092	140.964501
0195	38.759721	139.957373
0907	39.639369	141.426128
0134	42.699268	143.103257
0287	35.612086	137.174145
0937	37.669288	139.972663
0628	34.698904	138.939326
0105	44.728496	142.265247
0043	36.401847	139.726422
0010	42.963261	144.431936
0568	37.319871	139.020252
0504	44.191942	143.076819
0258	35.984908	136.504924
0598	34.239914	139.137575
0847	35.160451	137.868762
0166	39.596572	141.172105
0535	41.145546	140.821985
0817	35.066974	138.209984
0196	38.594037	139.831767
0783	44.148753	141.664599
0752	36.539259	139.056735
0135	42.667876	141.074955
0011	43.028625	143.459231
0044	36.697027	138.906264
0106	44.427048	141.330057
0569	37.056681	138.242586
0599	34.093764	139.561764
0848	45.514114	141.955250
0537	40.862361	141.131807
0753	36.003735	139.269328
0136	42.655530	141.602260
0784	43.722779	144.506409
0012	42.980515	142.401972

0939	37.461289	139.835523
0107	44.294568	142.625589
0169	39.338056	141.534158
3031	35.415350	139.045179
0570	36.950871	137.893871
0506	43.908405	142.577715
0260	35.792782	136.197394
0600	34.075781	139.478805
0819	34.902051	137.946810
0849	45.230106	141.881787
0198	37.963607	140.093526
0879	43.171330	143.027763
0910	39.235375	141.311673
0538	40.706276	140.589225
0170	39.253519	141.798042
0137	42.646290	140.825684
0785	43.624329	141.370584
0631	34.984394	136.862749
0046	36.499766	137.851122
0940	37.444871	140.464031
0971	37.432258	137.033941
3065	35.610274	139.157225
3001	36.295162	139.542301
0230	35.268600	139.142414
0507	43.828078	144.115255
0601	33.884124	139.612852
0171	39.023782	141.739846
0820	34.849413	138.176745
0199	38.197543	140.077573
0850	44.990504	142.292258
0788	43.101691	143.901986
0138	42.551647	143.461144
0172	38.902859	141.572589
0109	44.019183	145.186094
0941	37.326210	139.686345
0972	37.226436	136.908772
0014	42.983253	141.730671
3066	35.428518	139.204867
0231	38.465392	139.253348
3002	36.263269	140.174264
0508	43.738523	142.409610
0572	36.736958	137.369515
0602	32.463502	139.764616
1158	37.000719	136.772705
0821	34.752041	137.680777
0851	44.916065	142.021781
0881	43.149392	144.496498

0912	38.995463	141.148523
0293	35.261967	137.405606
0789	43.013652	142.870059
0540	40.624345	140.478527
0048	35.590335	138.583298
0139	42.549801	141.361481
0110	44.006778	142.151690
3067	35.267094	139.664837
0015	42.321594	143.331004
0942	37.293041	140.212745
0263	35.855978	138.316396
0232	38.319346	138.513087
0973	36.537266	136.540675
3003	36.203672	139.810527
1129	34.603334	136.431937
0573	36.649562	137.031898
0174	38.748937	140.801635
0509	43.740840	141.873847
0326	34.869327	136.054828
0822	35.300837	136.788824
0201	37.560553	140.755075
0882	43.140396	141.203293
0790	42.933772	142.084600
0294	35.227906	136.593445
0913	38.934027	140.833189
0758	35.616428	139.369897
0111	44.005620	143.333701
3068	35.245516	139.049338
0016	42.356904	142.364605
0943	37.210562	140.450970
0264	35.746875	138.695131
0974	36.229563	136.361645
0233	38.063279	138.471681
0510	43.771414	142.903019
0574	37.306970	137.138544
0202	37.566947	140.072680
0914	38.743220	141.317863
0791	42.806508	143.494972
0853	44.546500	142.571168
0542	40.910177	140.451565
0050	37.896470	138.988865
0759	35.160867	139.613842
0883	43.123895	143.597702
0141	42.481279	142.060223
0944	37.183092	140.715997
0017	42.450735	139.857668
3005	36.120951	139.345170

0234	37.929383	139.351465
0575	37.156744	136.718760
0511	43.670502	143.578155
0176	38.539480	141.147540
0915	38.686135	141.004335
0792	42.420548	141.081058
1101	35.104762	136.503757
0543	39.953080	141.066330
0113	43.549398	144.986963
0884	43.082596	140.811119
3070	35.496589	138.814037
0636	34.431442	136.628399
1162	38.511196	139.533822
0945	37.023581	140.376270
0204	37.473462	139.528628
0018	42.374215	140.942406
0606	35.649518	138.690381
0177	38.411756	140.851369
0235	37.815902	138.273068
0576	37.123156	136.996068
0512	43.232105	145.258951
0916	38.660630	141.160719
0297	34.865589	138.922254
0052	36.928958	137.487230
0544	39.351300	140.769184
0114	43.848897	143.787257
0793	42.486411	143.151974
0607	35.511868	139.025776
0205	37.325468	140.662112
0019	42.005856	143.156531
0267	36.665155	138.247467
0946	36.932620	140.690150
0977	35.888217	136.339579
0236	37.685906	139.477888
0577	36.817478	136.755651
0513	43.438836	144.079621
0546	39.143088	141.575489
0179	38.029659	140.843988
0053	37.382375	136.889166
0856	44.260854	143.364587
0115	43.661823	145.131435
0886	42.800343	143.655538
1008	34.493872	136.173149
0794	41.934853	140.371234
0638	35.420357	136.264746
0144	42.130936	142.935389
0608	36.239029	137.984550

0020	42.153546	139.519600
0947	36.475850	140.385691
0547	39.596124	141.675287
0268	36.386176	138.322523
0578	36.370069	136.605333
0180	37.989930	140.442574
0514	43.336265	142.395347
0237	37.667523	138.780505
0054	36.663412	136.649940
0299	35.190106	136.828832
0548	38.546216	140.847874
0116	43.408688	144.774327
0857	44.165474	142.400900
0795	39.849017	141.452591
3073	35.289461	138.445699
0887	42.803340	142.953686
0609	36.228369	137.871750
0021	42.008075	140.107324
0269	36.346013	138.637796
0579	35.968887	136.184992
0181	40.325047	140.577349
0515	43.307009	144.597660
0238	37.662295	139.059120
0549	38.425057	141.212910
0300	35.138752	137.253563
0919	38.177119	140.943689
0055	36.231172	136.172974
0117	43.404680	141.431175
0364	34.567032	136.050386
3074	35.200979	138.253514
0796	39.127008	140.988456
0858	44.114449	142.601247
0888	42.685336	140.011777
0022	41.826073	140.747826
0980	35.753871	138.949989
0270	36.322371	137.902815
0580	35.836841	136.055983
0949	36.872247	139.505314
0516	43.248411	141.890933
0182	40.271156	140.263661
0239	37.467718	138.998010
0920	37.824600	140.727664
0797	37.984407	140.645637
0301	35.039465	137.313164
1106	34.297927	136.388492
0118	43.382527	145.114961
0210	37.126294	140.259928

0147	42.042968	140.805541
0859	44.065033	144.993504
0023	41.466377	140.040652
0889	42.673963	143.312796
0271	36.208467	138.216485
0981	35.467692	138.606868
0611	36.084663	137.682627
0551	39.891134	139.848935
0517	43.209509	140.860617
0183	40.215440	140.787335
0950	36.537633	139.752790
0240	37.311315	138.789982
0799	38.434342	140.094631
1107	33.932948	136.139969
3044	35.111861	140.079268
0860	44.052106	141.860750
0272	36.130639	138.460973
0149	41.599025	140.315890
0024	41.300772	141.213275
0890	42.554262	142.395924
0582	36.300705	139.987766
0612	36.026163	138.214484
0184	40.247295	140.048679
0241	37.231122	138.333571
0800	37.018449	140.841646
0120	43.292584	140.597072
0212	36.862093	140.413270
0185	40.006878	140.401988
0273	36.121109	137.983011
0983	36.706647	138.096727
0150	41.455298	140.880506
0026	40.778984	140.272982
0861	43.909926	143.534157
0553	39.702681	140.732849
0583	36.114813	139.931499
0519	43.195165	145.520496
0059	35.800483	137.248373
0801	37.036934	139.402233
0952	36.837355	139.060852
0242	37.166035	138.933720
0121	43.289471	143.562424
0213	36.650567	140.293423
0274	35.783618	137.696260
0027	40.133449	141.789096
0554	39.199096	140.506691
0520	43.077589	141.540116
0151	41.043221	140.635892

0802	36.778061	138.944817
3047	34.954084	139.864078
0243	37.160790	138.100191
0954	36.591377	138.847891
0924	39.921391	140.535855
0028	39.572385	141.939962
0122	43.232934	144.325031
0214	36.800309	140.753912
0275	35.556130	138.038317
3079	35.103911	138.134901
0187	39.749162	140.597045
0615	35.726293	137.983889
0555	39.015972	139.927495
0863	43.878722	143.176695
0521	42.938860	143.170567
0893	41.711325	140.535026
0152	40.968244	141.367963
0803	38.288982	140.199916
0244	37.079132	138.608723
0029	39.110624	141.203919
3015	35.803329	140.407007
0955	36.395346	139.016710
0123	43.231993	143.298020
0215	36.364912	140.077947
0925	39.527565	140.053927
1174	40.575183	140.294993
0188	39.658309	140.234213
0586	36.979581	139.805748
0616	35.343734	137.676399
0556	38.496769	140.365152
0864	43.794028	145.056862
0986	35.944601	137.785436
0804	35.419268	139.521923
0153	40.625070	141.197831
0522	42.884431	141.577417
0245	37.045173	137.873847
3049	34.916115	138.924823
0030	39.967903	139.776150
0277	35.317144	137.925272
0216	36.344369	140.476333
0124	43.120607	144.126529
0189	39.549292	140.386625
1175	40.921155	140.990227
0587	36.776371	139.854257
0063	35.128109	137.041285
0557	38.148096	140.271138
0805	37.828158	139.226038

0154	40.577642	139.928117
0523	42.773190	141.407093
0246	36.993459	138.830845
0031	39.398697	140.048241
0278	35.246999	137.587668
0217	36.854234	140.039256
1144	34.970567	138.794657
3085	34.776075	138.786062
0125	43.057595	144.843024
1176	37.336698	140.808446
0618	36.285642	137.363020
0559	37.615952	140.205652
0988	35.815553	137.450879
0155	40.523654	140.578148
0806	37.776990	138.880441
0866	43.710323	143.381084
0525	42.551380	140.767623
0896	41.160934	141.385693
0247	36.865404	138.198674
0279	36.335510	137.147172
0032	38.894603	139.808852
0218	36.665983	139.619247
0126	43.056828	140.499172
1145	38.901934	141.283192
3019	35.710371	139.488263
0619	35.911634	137.200668
0156	40.515359	141.511282
0526	42.473902	140.876372
0897	41.121723	140.293529
0807	37.498656	138.779540
0280	36.033048	136.952763
0219	36.598946	139.923466
0311	34.547047	136.550657
3088	34.939797	138.074862
0127	42.985252	140.543938
0959	35.143803	139.968470
0620	34.855033	138.776523
0929	39.054380	140.447334
0590	36.542216	140.179308
0561	37.424507	140.135877
0157	40.291075	141.076475
0527	42.060505	139.446149
0249	36.634336	137.195197
0868	43.644561	143.991734
0220	36.769692	139.224904
0281	35.973458	137.534867
3053	34.751349	138.989815

0312	34.433140	136.334258
0991	35.723488	136.784620
0930	38.938103	140.183474
0591	36.616317	138.591445
0158	40.405200	141.713135
0250	36.578705	137.439896
0810	37.589737	138.920278
0528	42.123143	140.666868
0869	43.555994	145.220367
3090	34.941345	137.817940
0961	37.540342	139.111448
0842	34.954346	138.249899
0992	35.523129	137.309093
0564	38.056183	139.461685
0592	36.234670	139.066641
0901	40.508759	141.331994
0529	41.976687	140.715436
0870	43.545927	144.719044
2005	43.528644	141.844819
0871	43.521577	142.187612
1150	42.557933	140.898795
0594	34.761544	139.434017
0844	40.834407	140.810538
0933	38.628414	140.220506
0778	45.219767	141.598230
0813	35.114167	138.973867
0903	40.271043	141.484864
3059	34.121068	139.503849
3093	34.715251	138.053542
0964	37.107085	138.457359
0934	38.170440	140.393881
0845	37.361823	140.324390
0779	45.126774	142.351840
3060	34.059111	139.547153
0873	43.473581	143.753855
0965	36.778956	140.296488
0996	34.917341	137.152388
0905	39.970955	141.662180
0935	37.920585	139.879406
0966	36.919508	137.026432
0967	36.864344	137.551326
3097	34.792836	137.791792

Table S3. Locations of GEONET GPS stations used in analysis of Tohoku-oki earthquake.